# Technical Notes and Correspondence

## Nonlinear $H_\infty$ Controllers for Electromagnetic Suspension Systems

P. K. Sinha and A. N. Pechev

***Abstract*—This note presents a unified framework to derive nonlinear $H_\infty$ state and output feedback controllers for magnetically levitated (Maglev) vehicles with controlled dc electromagnets, referred to as electromagnetic suspension systems. The theoretical exposition, based on the Taylor series expansion solution to the Hamilton–Jacobi–Isaacs inequality, is followed by an assessment of some of the practical issues in realizing the nonlinear controllers with a digital signal processor and embedded hardware. A select set of experimental results from a single-degree-of-freedom suspension system is included to highlight the effectiveness of the proposed nonlinear state- and output-feedback $H_\infty$ controllers to suppress guideway-induced disturbances.**

***Index Terms*—$H_\infty$ controllers, digital signal processors, electromagnetic suspension systems, embedded control, Maglev, magnetic levitation, nonlinear systems.**

### I. Introduction

With the construction of the Shanghai city-Pudon international airport link in the Peoples Republic of China and the Hamburg–Berlin intercity route in Germany, magnetic levitation (Maglev) using electromagnetic suspension technology has come of age [1], [2]. The electromagnetic suspension (EMS) provides noncontacting suspension by means of dc electromagnets in conjunction with a position regulator using position (= airgap), velocity and acceleration feedback. Linear control theories have provided much of the benchmark design procedures for numerous full-scale vehicles in large test facilities [3]. However, due to constraints of linearization, the resulting time- and frequency-domain controllers have restricted capability to cope with significant changes in the suspended load (payload and disturbance force) or large variations in the guideway profile. An adaptive controller to compensate for payload variations and external force disturbances has been presented earlier [4]. This note develops a unified account for the derivation of nonlinear $H_\infty$ state and output feedback controllers to attenuate the effects of guideway-induced oscillations on suspension stability of the EMS system.

### II. Nonlinear Model of the EMS System

A schematic of a single-degree-of-freedom suspension system with a controlled dc electromagnet is shown in Fig. 1. The vehicle module, with its suspension magnet and payload (total mass $m$), travels under the fixed reaction surface (track or guideway); the linear propulsion motor is not shown in this illustration. Using the notations given in Fig. 1, the vertical dynamics is described by [3]

$$\begin{aligned} m\frac{d^2z(t)}{dt^2} &= -F(i,z,t)+f_d+mg \\ &= -\frac{\mu_0 N^2 a_m}{4}\left[\frac{i(t)}{z(t)}\right]^2+f_d+mg \\ \frac{di(t)}{dt} &= \frac{i(t)}{z(t)}\frac{dz(t)}{dt}-\frac{2}{\mu_0 N^2 a_m}z(t)(\mathrm{R}_m i(t)-u(t)). \end{aligned} \tag{1}$$

Defining a state vector $x(t)=[\,z(t)\quad \dot{z}(t)\quad i(t)\,]^T\in\Re^n$, $n=3$ and an external disturbance vector $w(t)=[\,w_1(t)\quad w_2(t)\,]^T,\in\Re^l$, $l=2$, (1) yields the following nonlinear state-space model of the open-loop suspension system:

$$\begin{aligned} \begin{bmatrix}\dot{x}_1(t)\\ \dot{x}_2(t)\\ \dot{x}_3(t)\end{bmatrix} &= \begin{bmatrix} x_2(t) \\ -\left(\frac{\mu_0 N^2 a_m}{4m}\right)\left[\frac{x_3(t)}{x_1(t)}\right]^2 \\ \frac{-2\mathrm{R}_m}{\mu_0 N^2 a_m}x_1(t)x_3(t)+\frac{x_2(t)x_3(t)}{x_1(t)}\end{bmatrix} \\ &\quad+\begin{bmatrix}0 & 0\\ \frac{1}{m}\alpha_1 & 0\\ 0 & 0\end{bmatrix}\begin{bmatrix}w_1(t)\\ w_2(t)\end{bmatrix}+\begin{bmatrix}0\\ 0\\ \frac{2}{\mu_0 N^2 a_m}x_1(t)\end{bmatrix}u(t) \\ \dot{x}(t) &= A(x(t))+B_1(x(t))w(t)+B_2(x(t))u(t) \end{aligned} \tag{2a}$$

$$\begin{aligned} y(t) &= [\,1\quad 0\quad 0\,]\begin{bmatrix}x_1(t)\\ x_2(t)\\ x_3(t)\end{bmatrix}+[\,0\quad \alpha_2\,]\begin{bmatrix}w_1(t)\\ w_2(t)\end{bmatrix} \\ &= C_2x(t)+D_{21}w(t) \end{aligned} \tag{2b}$$

with $\alpha_1$ and $\alpha_2$ as gains of the two disturbance inputs: $w_1(t)$ [= force disturbance, $f_d$] and $w_2(t)$ [= track or guide way disturbance, $z_{\mathrm{track}}(t)$]. While a predefined stability margin around a nominal operating point ($i_0$, $z_0$) is readily provided by a linear state feedback control law of the form ($z_{\mathrm{ref}}$ = reference airgap)

$$u(t)=k_p\{x_1(t)-z_{\mathrm{ref}}\}+k_v x_2(t)+k_a x_3(t) \tag{3}$$

where $k_p$ influences the steady-state error and hence stiffness, $k_v$ controls suspension damping and $k_a$ overall stability margin, linear controllers have limited ability to suppress guideway-induced disturbances. The track oscillating mechanism in the experimental rig shown in Fig. 1 has specifically been added to emulate vertical movement of the guideway as the vehicle travels along. The analytical derivations presented in this note demonstrate that the $H_\infty$ control methodology offers a convenient design framework to deal with the effects of such external disturbances with respect to a user-defined penalty vector $q(t)\in\Re^{n+1}$ (Fig. 2)

$$\begin{aligned} q(t) &= \begin{bmatrix}q_1\\ q_2\\ q_3\\ q_4\end{bmatrix}=\begin{bmatrix}\beta_1 & 0 & 0\\ 0 & \beta_2 & 0\\ 0 & 0 & \beta_3\\ 0 & 0 & 0\end{bmatrix}\begin{bmatrix}x_1\\ x_2\\ x_3\end{bmatrix}+\begin{bmatrix}0\\ 0\\ 0\\ W_u\end{bmatrix}u \\ &= C_1x+D_{12}u \end{aligned} \tag{4}$$

where $W_u$ is a weight on the control signal and $C_1\in\Re^{(n+1)\times n}$ is a scaling matrix chosen to define the relative influence of the state variable in the construction of the penalty vector. The objective of the non-

Manuscript received April 18, 2002; revised December 16, 2002. Recommended by Associate Editor K. M. Grigoriadis. Equipment and software support from Analog Devices and financial support from Jupelier Technology during this basic research project are gratefully acknowledged.

P. K. Sinha is with the Department of Engineering, The University of Reading, Reading RG6 6AY, U.K. (e-mail: p.k.sinha@rdg.ac.uk).

A. N. Pechev is with the Cardiff School of Engineering, Cardiff University, Cardiff CF24 0YF, U.K.

Digital Object Identifier 10.1109/TAC.2003.822865

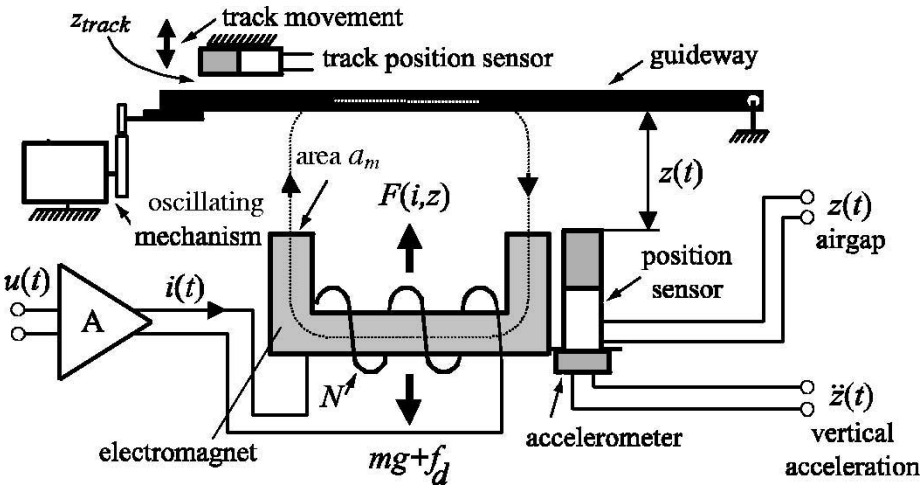


Fig. 1. Magnet-guideway configuration of the experimental system used in this note. Guideway disturbance is introduced by the oscillating mechanism on the top left corner. Notations: $m$ = mass; $f_d$ = force disturbance; $g$ = gravitational acceleration; $N$ = number of turns in the magnet winding; $a_m$ = magnet pole face area; $R_m$ = magnet winding resistance.

linear design procedure developed here is to identify a class of feedback controllers that satisfies the $\mathcal{L}_2$-gain inequality [5]

$$\int_0^T \|q(t)\|^2 dt \le \gamma^2 \int_0^T \|w(t)\|^2 dt, \qquad 0 \le \gamma \le 1 \tag{5}$$

by keeping the energy of the penalty vector $q(t)$ bounded and smaller than the energy of the disturbance input $w(t)$. Because of this bounded energy notion, the concepts of *dissipativity* and *storage function* [6], [7] are adopted here. It has been established that the equilibrium point of a dissipative dynamical system is stable if for $x(t)|_{t=0} = 0$, there exists a nonnegative smooth storage function $V(x(t))$ that satisfies the Hamilton–Jacobi–Isaacs (HJI) inequality [8], [9]

$$V_x(x)^T [A(x) + B_1(x)w + B_2(x)u] + [C_1 x + D_{12}u]^T [C_1 x + D_{12}u] - \gamma^2 w^T w \le 0 \tag{6}$$

(where $V_x(x) = \partial V(x(t))/\partial x(t)$; for notational simplicity, time $(t)$ is dropped in subsequent derivations). In subsequent derivations, the whole left-hand side of the HJI inequality is denoted as the Hamiltonian function $H[x, V_x(x), w, u]$. The premise of the proposed algorithm is that any feedback control law that satisfies the HJI inequality will yield a stable closed-loop system; i.e., the closed-loop system is locally dissipative with respect to its supply rate. As local dissipativity also implies the existence of storage function, the $H_\infty$ design in this context may be recast as the problem of deriving a class of control laws and their corresponding storage functions which satisfy (6)

## III. Nonlinear $H_\infty$ State Feedback

The general configuration of the closed-loop system is shown in Fig. 2, where the unknown disturbance inputs $w_1$ and $w_2$ are force and track disturbances with the penalty vector $q$ being defined in (4).

As the design criterion is to find $u(x)$ that satisfies the HJI inequality, the analytical derivations are focussed on finding a saddle point in the Hamiltonian function such that

$$H\left[x, V_x(x), w, \breve{u}\right] \le H\left[x, V_x(x), \widehat{w}, \breve{u}\right] \le H\left[x, V_x(x), \widehat{w}, u\right] \tag{7}$$

with $\widehat{w}$ as the worst disturbance input that maximizes $H(\bullet)$ and $\breve{u}$ as the control input that minimizes $H(\bullet)$. With $D = D_{12}^T D_{12}$ and $C_1^T D_{12} = 0$ for the Maglev model, these are given by [5], [8], [9]

$$\widehat{w} = \widehat{w}\{x, V_x(x)\} = \frac{1}{2}\gamma^{-2} B_1(x)^T V_x(x)$$
$$\breve{u} = \breve{u}\{x, V_x(x)\} = -\frac{1}{2} D^{-1} B_2(x)^T V_x(x). \tag{8a}$$

To compute the unknown storage function $V(x(t))$ that satisfies the above saddle point condition, (8a) is substituted into (6) to give the following HJI inequality:

$$H_*[x, V_x(x)] = V_x(x)^T A(x) - \breve{u}^T D\, \breve{u} + x^T C_1^T C_1 x + \gamma^2 \widehat{w}^T \widehat{w} \le 0. \tag{8b}$$

In the absence of an analytical solution, (8b) is transformed into an infinite sum inequality by Taylor series (originally proposed in [10]) with the $k^{th}$ power term as

$$V_x(x)^{[2]T} A(x)^{[k]} + \cdots + V_x(x)^{[k+1]T} A x^{[1]} - \breve{u}^{[1]T} D\, \breve{u}^{[k]} - \cdots - \breve{u}^{[k]T} D\, \breve{u}^{[1]} + x^T C_1^T C_1 x + \gamma^2 \left\{ \widehat{w}^{[1]T} \widehat{w}^{[k]} + \cdots + \widehat{w}^{[k]T} \widehat{w}^{[1]} \right\} \le 0 \tag{9}$$

where $Ax^{[1]}, A(x)^{[2]}, \ldots A(x)^{[k]}$ are the first, second, $\ldots, k^{th}$ terms in the Taylor series expansion of $A(x)$ in (2a). Application of the same power series expansion to (8a) gives the following generic relationships for the worst disturbance vector and the input control signal for any $k$th order term

$$\widehat{w}^{[k]} = \frac{1}{2}\gamma^{-2} \left\{ B_1^{[1]T} V_x(x)^{[k+1]} + \cdots + B_1(x)^{[k]T} V_x(x)^{[2]} \right\}$$
$$\breve{u}^{[k]} = -\frac{1}{2} D^{-1} \left\{ B_2^{[1]T} V_x(x)^{[k+1]} + \cdots + B_2(x)^{[k]T} V_x(x)^{[2]} \right\} \tag{10}$$

where $B_1^{[j]}, B_2^{[j]}$ and $V_x(x)^{[j+1]}, j = 1, \ldots k$, are the Taylor series expansion of the system in (1) and the storage function $V(x)$. The generic properties of these power series provide a mechanism to build up higher order controllers cumulatively, as given as follows for first- and second-order controllers.

a) **First-order controller**, $\breve{u} = \breve{u}^{[1]}$, with $\breve{u}^{[1]}$ given with $k = 1$ in (10)

$$\text{control input} \rightarrow \breve{u}^{[1]} = -\frac{1}{2} D^{-1} B_2^{[1]T} V_x(x)^{[2]} \tag{11a}$$

$$\text{worst disturbance vector} \rightarrow \widehat{w}^{[1]} = \frac{1}{2}\gamma^{-2} B_1^{[1]T} V_x(x)^{[2]} \tag{11b}$$

$$\text{HJI inequality} \rightarrow V_x(x)^{[2]T} A x^{[1]} - 2\breve{u}^{[1]T} D \breve{u}^{[1]} + 2\gamma^2 \widehat{w}^{[1]T} \widehat{w}^{[1]} + x^T C_1^T C_1 x \leq 0. \tag{11c}$$

b) **Second-order controller**, $\breve{u} = \breve{u}^{[1]} + \breve{u}^{[2]}$, where $\breve{u}^{[2]}$ is given with $k = 2$ in (10)

$$\breve{u}^{[2]} = -\frac{1}{2} D^{-1} \left[ B_2^{[1]} V_x(x)^{[3]} + B_2(x)^{[2]T} V_x(x)^{[2]} \right] \tag{12a}$$

$$\widehat{w}^{[2]} = \frac{1}{2}\gamma^{-2} \left[ B_1^{[1]T} V_x(x)^{[3]} + B_1(x)^{[2]T} V_x(x)^{[2]} \right] \tag{12b}$$

$$V_x(x)^{[2]T} A(x)^{[2]} + V_x(x)^{[3]T} A x^{[1]} - \breve{u}^{[1]T} D \breve{u}^{[2]} - \breve{u}^{[2]T} D \breve{u}^{[1]} + \gamma^2 \left\{ \widehat{w}^{[1]T} \widehat{w}^{[2]} + \widehat{w}^{[2]T} \widehat{w}^{[1]} \right\} \leq 0. \tag{12c}$$

### *A.* Numerical Results

To derive the above nonlinear $H_\infty$ state-feedback controllers, the Taylor-series-expansions for the Maglev system in (2) is derived as in (13a) for a nominal operating point $z_0 = 4.0 \times 10^{-3}$ m, $i_0 = 3.13$ A with $N = 280$, $m = 1.5$ kg, $a_m = 1.024 \times 10^{-2}\,\mathrm{m}^2$ and $\mathrm{R}_m = 1.1\,\Omega$

$$\begin{aligned} A(x) &= Ax^{[1]} + A(x)^{[2]} \\ &= \begin{bmatrix} 0 & 1 & 0 \\ \left(\frac{\mu_0 N^2 a_m}{2m}\right)\frac{i_0^2}{z_0^3} & 0 & -\left(\frac{\mu_0 N^2 a_m}{2m}\right)\frac{i_0}{z_0^2} \\ \left(\frac{-2\mathrm{R}_m}{\mu_0 N^2 a_m} - \frac{\dot{z}_0}{z_0^2}\right) i_0 & \frac{i_0}{z_0} & \left(\frac{-2\mathrm{R}_m}{\mu_0 N^2 a_m} + \frac{\dot{z}_0}{z_0}\right) \end{bmatrix} \begin{bmatrix} x_1 \\ x_2 \\ x_3 \end{bmatrix} \\ &\quad + \begin{bmatrix} 0 \\ -\frac{\mu_0 N^2 a_m}{4m}\left\{\frac{3i_0^2}{z_0^4}x_1^2 + \frac{1}{z_0^2}x_3^2 - \frac{4i_0}{z_0^3}x_1 x_3\right\} \\ -\frac{i_0}{z_0^2}x_1 x_2 + \left(\frac{-2\mathrm{R}_m}{\mu_0 N^2 a_m} - \frac{\dot{z}_0}{z_0^2}\right) x_1 x_3 + \frac{1}{z_0} x_2 x_3 + \frac{\dot{z}_0 i_0}{z_0^3} x_1^2 \end{bmatrix} \end{aligned}$$

$$B_1(x) = B_1^{[1]} + B_1(x)^{[2]} = \begin{bmatrix} 0 & 0 \\ \frac{1}{m}\alpha_1 & 0 \\ 0 & 0 \end{bmatrix} + 0;$$

$$B_2(x) = B_2^{[1]} + B_2(x)^{[2]} = \begin{bmatrix} 0 \\ 0 \\ \frac{2}{\mu_0 N^2 a_m} z_0 \end{bmatrix} + \begin{bmatrix} 0 \\ 0 \\ \frac{2}{\mu_0 N^2 a_m}[x_1 - z_0] \end{bmatrix};$$

$$D = D_{12}^T D_{12} = W_u^2. \tag{13a}$$

It can be shown that for a dissipative system to be stable, the storage function has the characteristic features of a Lyapunov function with a strong local minimum at the equilibrium point [6]. To derive $\breve{u}^{[1]}$, $V(x)^{[2]}$ is taken as the quadratic function $V(x)^{[2]} = x^T P x$, with $P > 0$ being unknown, the HJI inequality in (11c) then holds good if $P$ satisfies the Riccati equation in (13b)

$$H_{1*} = A^{[1]T} P + P A^{[1]} + P\left(\gamma^{-2} B_1^{[1]} B_1^{[1]T} - B_2^{[1]} D^{-1} B_2^{[1]T}\right) P + C_1^T C_1 = 0. \tag{13b}$$

Assigning the values $\alpha_1 = \alpha_2 = 1$, $\beta = I_3$, $W_u = 0.12$ and $\gamma = 1$ in the series expansion matrices shown previously, a solution of (13) (using Matlab algebraic Riccati equation routine) gives

$$P = \begin{bmatrix} 5.5198 \times 10^4 & 6.3994 \times 10^2 & -4.7601 \\ 6.3994 \times 10^2 & 7.5823 & -5.2934 \times 10^{-2} \\ -4.7601 & -5.2934 \times 10^{-2} & 1.0844 \times 10^{-3} \end{bmatrix}.$$

The corresponding first-order control law and the disturbance signals are then derived from (11) and given in (14).

$$\breve{u}^{[1]} = 262.13 \times 10^2 x_1 + 291.5 x_2 - 5.972 x_3 \tag{14a}$$

$$\widehat{w}^{[1]} = \begin{bmatrix} \widehat{w}_1^{[1]} \\ \widehat{w}_2^{[2]} \end{bmatrix} = \begin{bmatrix} 4.647 \times 10^4 x_1 + 5.534 x_2 - 3.822 \times 10^{-2} x_3 \\ 0 \end{bmatrix}. \tag{14b}$$

To derive the second-order controller, $\breve{u} = \breve{u}^{[1]} + \breve{u}^{[2]}$, $V(x)^{[3]}$ is defined as the cubic polynomial $V(x)^{[3]} = c_1 x_1^3 + c_2 x_1^2 x_2 + c_3 x_1^2 x_3 + \cdots + c_9 x_2 x_3^2 + c_{10} x_3^3$, where the unknown coefficients $\{c_i\}, i = 1..10$, are to be derived from the second-order HJI equation in (12c), rewritten as (15) with $V(x)^{[2]}$, $\breve{u}^{[1]}$ and $\widehat{w}^{[1]}$ taken from the first-order controller

$$V_x(x)^{[3]}\left(Ax^{[1]} + B_1^{[1]T}\widehat{w}^{[1]} + B_2^{[1]T}\breve{u}^{[1]}\right) x + V_x(x)^{[2]}\left(A(x)^{[2]} + B_1(x)^{[2]T}\widehat{w}^{[1]} + B_2(x)^{[2]T}\breve{u}^{[1]}\right) = 0. \tag{15}$$

Equating terms in (15) with equal powers leads to a set of ten equations. Solution of these equations using the Gauss–Seidel elimination method gives the values for the unknown coefficients $\{c_i\}, i = 1, \ldots, 10$ and hence the unknown storage function $V(x)^{[3]}$. With the parameters given earlier, the second-order controller in (11a) and (12a) becomes

$$\begin{aligned} \breve{u}(x) &= \{\breve{u}^{[1]}\} + \{\breve{u}^{[2]}\} \\ &= \{262.13 \times 10^2 x_1 + 291.5 x_2 - 5.972 x_3\} \\ &\quad - \{483.88 \times 10^3 x_1^2 - 574.38 \times 10^2 x_1 x_2 - 4392.37 x_1 x_3 \\ &\quad - 194.32 x_2^2 - 31.80 x_2 x_3 + 0.403 x_3^2\}. \end{aligned} \tag{16}$$

This second-order controller has been implemented on the experimental single-degree-of-freedom system; the controller's performance in attenuating track disturbance is discussed in Section VI.

## IV. Nonlinear $H_\infty$ Output Feedback

Although all state variables are available for feedback in a Maglev vehicle suspension system, results Section III are extended to output feedback for two reasons: a) use of $H_\infty$ controllers to other applications, such as magnetic bearings which usually employ only position sensors; and b) provide a basis for further work related to sensor fault accommodation [11]. The output feedback control law derived here uses a state estimator in conjunction with the same state-feedback control law in (16). For uniformity in the design procedure, the nonlinear state estimator [(17)] is derived using the concept of local dissipation described earlier [9].

$$\begin{aligned} \dot{\tilde{x}} &= A(\tilde{x}) + B_1(\tilde{x}) w + B_2(\tilde{x}) u + Q(\tilde{x})(y - \tilde{y}) \\ \tilde{y} &= C_2 \tilde{x} + D_{21} w \end{aligned} \tag{17}$$

where $\tilde{x}$ is the estimator state vector and $\tilde{y}$ is the estimator output. In general, the unknown *output gain* $Q(\tilde{x})$ has a nonlinear structure; an approximate solution maybe derived by using the same procedure based on Taylor series expansions as in Section IV. The corresponding first-order solution for $Q^{[1]}$ is then derived as [9]

$$(R - P) Q^{[1]} = \left(D_{21} D_{21}^T\right)^{-1} \left(D_{21} B_1^{[1]T} R + \gamma^2 C_2^T\right) \tag{18a}$$

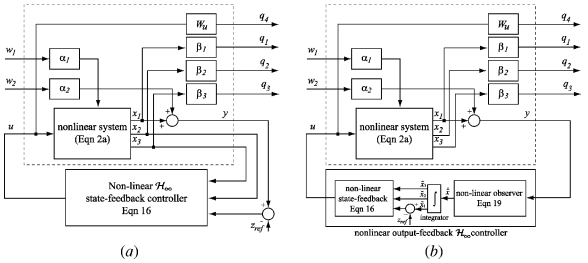


Fig. 2. (a) State-feedback and (b) output-feedback control configurations.

where $P$ defines the storage function $V(x)^{[2]}$ as computed in the state feedback controller derivation and $R$ is the solution of the following Riccati equation:

$$\left(A^{[1]} - B_1^{[1]} D_{21}^T \left(D_{21} D_{21}^T\right)^{-1} C_2\right)^T R + R\left(A^{[1]} - B_1^{[1]} D_{21}^T \left(D_{21} D_{21}^T\right)^{-1} C_2\right) + R\left(\gamma^{-2} B_1^{[1]} B_1^{[1]T} - B_1^{[1]} D_{21}^T \left(D_{21} D_{21}^T\right)^{-1} D_{21} B_1^{[1]T}\right) R + C_1^T C_1 - \gamma^2 C_2^T \left(D_{21} D_{21}^T\right)^{-1} C_2 - H_{1*} = 0 \quad (18b)$$

with $H_{1*}$ as defined on the left-hand side of (13b). For the Maglev system with parameters in Fig. 1 and the value of $P$ as computed in Section III.A, the solutions for $R$ and $Q^{[1]}$ are derived as

$$R = \begin{bmatrix} 9.6628 \times 10^{11} & -2.8380 \times 10^{7} & -9.3912 \times 10^{8} \\ -2.8379 \times 10^{7} & 2.4514 \times 10^{4} & -1.2372 \times 10^{5} \\ -9.3912 \times 10^{8} & -1.2372 \times 10^{5} & 2.4921 \times 10^{6} \end{bmatrix}$$

and

$$Q^{[1]} = \begin{bmatrix} 8.1733 \times 10^{3} \\ 33.401 \times 10^{6} \\ 47.382 \times 10^{5} \end{bmatrix}$$

with the corresponding state estimator given by (19), as shown at the bottom of the page. Solution of these nonlinear equations gives the estimated state variables $\tilde{x}_1$, $\tilde{x}_2$ and $\tilde{x}_3$ which are then used in (16) to implement the output feedback controller using the configuration in Fig. 2(b); performance of the resulting controller is discussed in Section VI.

## V. Control Hardware

As part of a hardware design project for commercial Maglev vehicles and magnetic bearings, an Analog Devices Sharc 21 062 DSP-based embedded controller hardware has been manufactured by the authors and their industrial collaborators [12]. It integrates Ethernet/TCP/IP communication facilities and software functions for real-time communication with Matlab/SIMULINK environment. The sampling time has been chosen to be 1 ms for compatibility with the typical inductance values of the windings of suspension magnets and the cut-off frequency of the anti-aliasing filter set at 25 kHz [$= (1/2)$ of per-channel sampling rate of ADC]. The main tasks performed in each sample are: data capture and conversion (including integration of the acceleration signal to generate velocity), execution of the control law, outputting of the control signal and storing data for offline analysis (the embedded hardware offers up to 4 Mbytes of onboard RAM). Each sample is interrupt-driven from the internal timer of the DSP. The software written in C/assembler for SHARC DSP's offers facilities to serve host-based Matlab visualization. The analogue processing tasks consume 5% to 8% of the sampling time and the nonlinear state-feedback ((16)) a further 5%–40%, the remainder being used to serve the host.

To implement an output-feedback controller (state estimator + state-feedback controller) on an embedded hardware, the classical linear control would require a transformation from the continuous time-domain to a discrete time-domain. Because of the nonlinear nature of the observer [(19)], this procedure is inapplicable. The scheme adopted here to overcome this limitation is to include a Runge–Kutta solver within the control loop. In doing so at every sample, the software on the DSP reads the most recent output of the system and multiplies it by the output injection gain $Q^{[1]}$. The set of first-order differential equations in (19) is then integrated by a dedicated Runge-Kutta-4 integration routine. For satisfactory convergence of this integration process, experience suggested that around 50 steps, each of length $h = 10^{-5}$, are typically required for reasonable estimation of the state vector $\tilde{x}_{50} = [\,\tilde{x}_1 \quad \tilde{x}_2 \quad \tilde{x}_3\,]_{50}^T$. At the end of the 50th step, final values of these three state variables are taken as the input to the nonlinear state-feedback controller ((16)). The full collection of software tasks for nonlinear output-feedback control takes around 400 $\mu$s per cycle; the remaining 600 $\mu$s of the sampling time is available to serve the host.

## VI. Experimental Results

The oscillating mechanism in Fig. 1 is capable to introducing step change as well as periodic motion of the guideway. The vertical profile of the guideway is measured by a noncontacting position sensor mounted on a fixed datum. Fig. 3 shows responses of the suspension system with a step change in the guideway position ($z_{\mathrm{track}}$) and a step change in the reference airgap ($z_{\mathrm{ref}}$) for three types of controllers: linear state-feedback, second order nonlinear state-feedback and the nonlinear output-feedback. The first-order nonlinear state-feedback control law in (14a) was also implemented, but as the corresponding step responses almost overlapped with those with the linear state-feedback control law in (3), they are not included. The responses in Fig. 3 indicate that the new nonlinear controllers improve the overall settling time almost by a factor of two, compared with the conventional linear state feedback controller. The reduction in overshoots in Fig. 3 (curve-3) indicates that, within the definitions of linear systems, peak amplitude in the sensitivity function will remain below the 0-dB boundary. To study this further, a series of experiments was carried out with sinusoidal variations in the guideway position. At each run, the system is suspended at a fixed $z_{\mathrm{ref}}$, the track is oscillated and the airgap and the guideway positions recorded. Fourier analysis is then performed on these data to determine the fundamental frequency of the guideway profile and the attenuation rate of the airgap error ($z_{\mathrm{ref}} - z$). Initially, these experiments were performed with a linear state-feedback controller ((3)); the corresponding response for the highest frequency is shown in Fig. 4 (top, with attenuation rates as given). These experiments were repeated over the whole of the

$$\begin{bmatrix} \dot{\tilde{x}}_1 \\ \dot{\tilde{x}}_2 \\ \dot{\tilde{x}}_3 \end{bmatrix} = \begin{bmatrix} -8173.3\tilde{x}_1 + \tilde{x}_2 + 8173.3y \\ -33.4 \times 10^6 \tilde{x}_1 + 7.99\tilde{x}_2 + 159 \times 10^{-3}\tilde{x}_3 + 0.168 \times 10^{-4}\frac{\tilde{x}_3^2}{\tilde{x}_1^2} + 33.4 \times 10^6 y \\ -4738.2 \times 10^3 \tilde{x}_1 + 0.7508 \times 10^7 \tilde{x}_1\tilde{x}_2 - 151.461 \times 10^7 \tilde{x}_1\tilde{x}_3 + 0.5406 \times 10^9 \tilde{x}_1^2 + \frac{\tilde{x}_2\tilde{x}_3}{\tilde{x}_1} + 47.382 \times 10^5 y \end{bmatrix}. \quad (19)$$

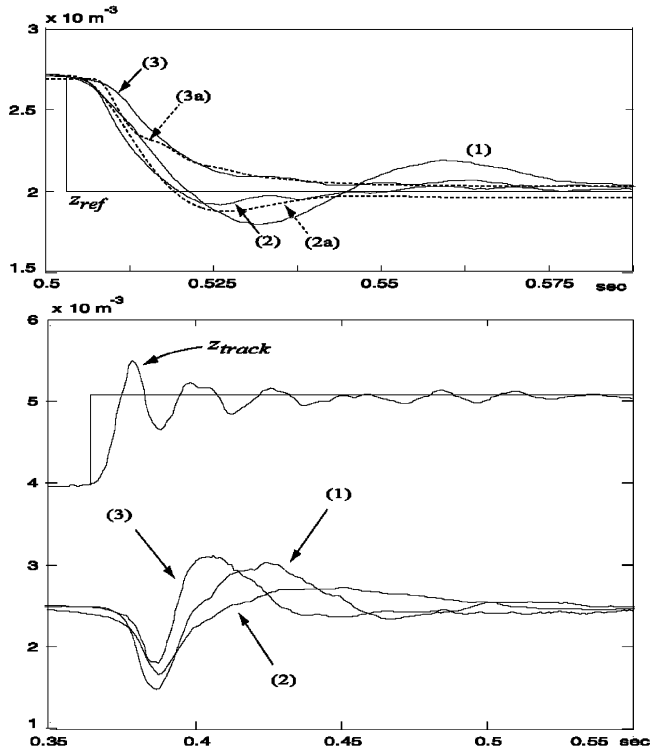


Fig. 3. Experimental and simulation transient responses. Top: step change in airgap reference $z_{\rm ref}$ from 2.75 mm to 2.0 mm with clamped guideway. (1) Linear state-feedback controller (3) with $k_p = 207.923$, $k_v = 1.5$ and $k_a = 0.00424$. (2) Experimental responses with nonlinear state-feedback controller (16) and (2a) the corresponding simulation response. (3) Experimental response with nonlinear output-feedback controller (16) and (19) and (3a) the corresponding simulation response. Nominal operating conditions for all controllers are $i_0 = 3.13$ A and $z_0 = 4.0$ mm. Bottom: Experimental responses due to a step change in guideway position ($z_{\rm ref}$ kept constant at 2.5 mm) with controller parameters as above.

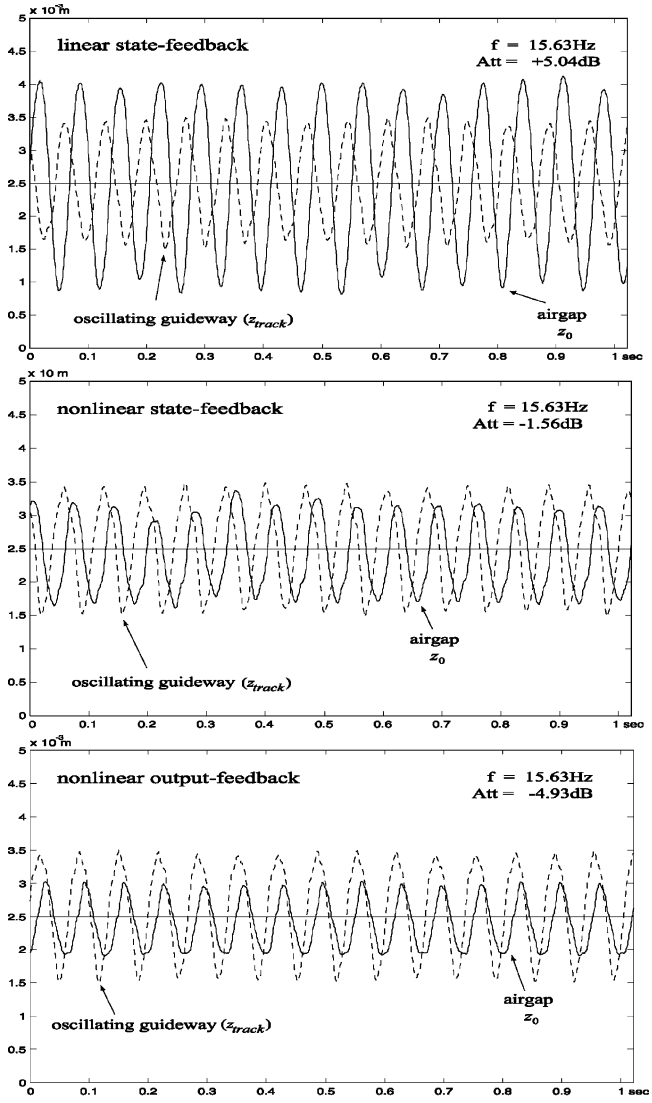


Fig. 4. Experimental responses with sinusoidally oscillating track. Top: linear state-feedback controller (3); middle: nonlinear second-order state-feedback controller (16); bottom: nonlinear output-feedback $H_\infty$ controller (16) and (19).

frequency range for which the system maintained a stable suspension and the corresponding sensitivity function (curve-1) is plotted in Fig. 5; bandwidth of the closed-loop system with linear state feedback controller was observed to be around 9.5 Hz with the peak value of its sensitivity function being 6 dB. Consequently, disturbances with frequencies $\approx 15$ Hz will be amplified nearly by a factor of two, leading to an unacceptable operation (airgap error rising up to two times the guideway variation). Although there was insignificant difference between the step responses of the linear state feedback and the nonlinear first-order state feedback controllers, the latter was seen to have a narrower bandwidth but a lower peak (curve-2 in Fig. 5). The above sequence of operations was also performed with the nonlinear second-order state-feedback controller and the nonlinear output-feedback controller over the same range of frequencies. The corresponding responses for 15.63 Hz are shown in Fig. 4 (middle and bottom). The respective experimentally derived frequency responses are marked as curves 3 and 4 in Fig. 5. To provide a basis for comparison with theoretical results, frequency responses with nonlinear state feedback and output feedback controllers from simulation studies have been included in Fig. 5 (dotted lines). These, along with the simulated step response in Fig. 3, underline the overall effectiveness of the proposed control architecture.

Two specific observations may be made from the shapes of the sensitivity function (Fig. 5): a) bandwidth is increased, giving increased attenuation in the low-frequency range; and b) the increase in energy on the output remains bounded by $\gamma = 1$ and hence the inequality in (5) is satisfied. Consequently, at low frequencies ($< 10$ Hz) the magnet will follow the guideway profile satisfactorily and at higher frequencies it would still remain below the amplitude of the guideway movement (measured from its datum line). As the permissible peak variation in the guideway is closely related to the mean operating airgap, this implies that the second order state-feedback and the output-feedback nonlinear $H_\infty$ controllers are capable of maintaining a stable suspension over a wider frequency range than their linear counterpart.

## VII. Conclusion

While the linear state feedback controllers have successfully been used over the years, the new experimental results presented here demonstrate the viability of using more computationally demanding nonlinear controllers for stabilization and control of electromagnetic suspension systems. The superiority of the second-order state feedback and the output feedback controllers in tracking a moving guideway with improved disturbance rejection properties has been illustrated. While both nonlinear controllers improve suspension characteristics, the output feedback controller (which subsumes a nonlinear state estimator) has been observed to provide significant improvement over

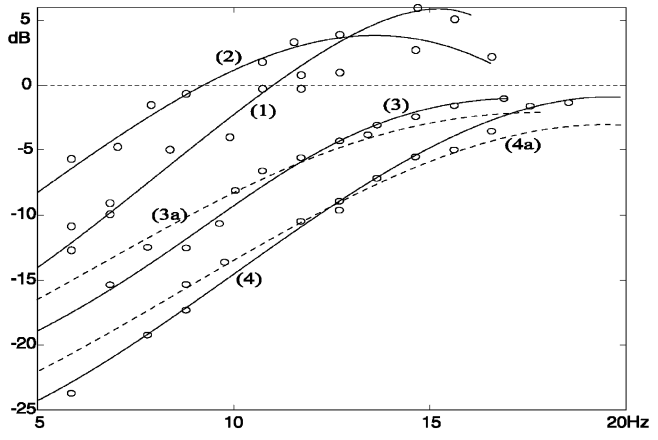


Fig. 5. Experimental and simulation sensitivity functions of the closed-loop system. (1) Linear state-feedback controller (3), (2) first-order nonlinear state-feedback controller (14a), (3) second order nonlinear state-feedback controller (16) and (4) nonlinear output-feedback controller (16) and (19). (3a) and (4a) represent the simulation responses corresponding to (3) and (4). The value of $W_u$ puts a penalty on the control signal; small values of $W_u$ lead to faster transient response and, hence, wider bandwidth. In all responses contained in this note $\gamma$ and $W_u = 0.12$.

the now-classical linear state feedback controllers. The concept of linear $H_\infty$ [13] has been used for Maglev control [14], [15] earlier, however, direct application of nonlinear $H_\infty$ to deal with track disturbance in an EMS system is considered to be novel.

Although several issues require careful assessment for the real-time implementation of these nonlinear $H_\infty$ controllers derived here, extensive range of experimental work carried out by the authors indicate that, providing a reasonable care is taken in specifying the physical parameters of the suspension magnet, the analytically derived control laws, for a given set of $\alpha$, $\beta$, $\gamma$ and $W_u$, may directly be used in assessing the performance of laboratory-scale demonstration systems. A key difference between the nonlinear state and the output feedback controllers is the execution time of the control algorithms ((16) and (19)): 50 $\mu$s for the former and 400 $\mu$s for the latter (within a sampling interval of 1 ms). In multimagnet vehicles this may impose some operational constraints. To overcome this, the embedded DSP hardware described in Section V provides communication protocols between local control loops for individual magnets and supervisory control functions to coordinate the distribution of suspension force. The dynamics of these mechanically coupled magnets on suspension stability and tracking properties are currently under investigation.

## REFERENCES

[1] *The Economist: "The New Age of the Train: A Better Way to Fly"*, The Economist, London, U.K., 1998, pp. 23–25.
[2] *The Shanghai-Pudon Airport Highspeed Link*, Transrapid International, Berlin, Germany, 2001.
[3] P. K. Sinha, *Electromagnetic Suspension: Dynamics & Control*. London, U.K.: Peter Peregrinus, 1987.
[4] P. K. Sinha and A. N. Pechev, "Model reference adaptive control of a Maglev system with stable maximum descent criterion," *Automatica*, vol. 35, pp. 1457–1465, 1999.
[5] A. J. van der Schaft, "$L_2$-gain analysis of nonlinear systems and nonlinear state feedback $H_\infty$ control," in *IEEE Trans. Automat. Contr.*, vol. 37, June 1992, pp. 770–784.
[6] J. G. Willems, "Dissipative dynamical systems Part I: General theory," *Arch. Rational Mech. Anal.*, vol. 22, pp. 321–351, 1972.
[7] D. Hill and P. Moylan, "The stability of nonlinear dissipative systems," *IEEE Trans. Automat. Contr.*, vol. AC-21, pp. 708–711, June 1976.
[8] J. A. Ball, J. Helton, and M. L. Walker, "$H_\infty$ control for nonlinear systems with output feedback," *IEEE Trans. Automat. Contr.*, vol. 38, pp. 546–559, May 1993.
[9] A. Isidori and W. Kang, "$H_\infty$ control via measurement feedback for general nonlinear systems," *IEEE Trans. Automat. Contr.*, vol. 40, pp. 466–472, Mar. 1995.
[10] E. G. Al'brekht, "On the optimal stabilization of nonlinear systems," *J. Appl. Math. Mech.*, vol. 25, pp. 1254–1266, 1962.
[11] P. K. Sinha, F. B. Zhou, and R. S. Kutiyal, "Fault detection in electromagnetic suspension systems with state estimation methods," *IEEE Trans. Magn.*, vol. 29, pp. 2971–2973, Dec. 1993.
[12] *"Sharc DSP Board for Embedded Control" Data Sheet*, Jupelier Technology, Hamm, Germany, 2000.
[13] J. C. Doyle, K. Glover, P. Khargonekar, and B. Francis, "State-space solutions to standard $H_2$ and $H_\infty$ control problems," *IEEE Trans. Automat. Contr.*, vol. 34, pp. 831–847, Aug. 1989.
[14] A. Bittar and R. M. Sales, "$H_2$ and $H_\infty$-control for maglev vehicles," *IEEE Control Syst. Mag.*, vol. 18, pp. 18–25, Jan. 1998.
[15] M. Fujita, T. Namerikawa, F. Matsumura, and K. Uchida, "$\mu$-synthesis of an electromagnetic suspension system," *IEEE Trans. Automat. Contr.*, vol. 40, pp. 530–536, Apr. 1995.

# Robust Stability and Stabilization of Discrete Singular Systems: An Equivalent Characterization

Shengyuan Xu and James Lam

***Abstract*—This note deals with the problems of robust stability and stabilization for uncertain discrete-time singular systems. The parameter uncertainties are assumed to be time-invariant and norm-bounded appearing in both the state and input matrices. A new necessary and sufficient condition for a discrete-time singular system to be regular, causal and stable is proposed in terms of a strict linear matrix inequality (LMI). Based on this, the concepts of generalized quadratic stability and generalized quadratic stabilization for uncertain discrete-time singular systems are introduced. Necessary and sufficient conditions for generalized quadratic stability and generalized quadratic stabilization are obtained in terms of a strict LMI and a set of matrix inequalities, respectively. With these conditions, the problems of robust stability and robust stabilization are solved. An explicit expression of a desired state feedback controller is also given, which involves no matrix decomposition. Finally, an illustrative example is provided to demonstrate the applicability of the proposed approach.**

***Index Terms*—Discrete-time systems, linear matrix inequality (LMI), parameter uncertainty, robust stability, robust stabilization, singular systems.**

## I. INTRODUCTION

The problems of robust stability analysis and robust stabilization of linear state-space systems with parameter uncertainties have received much attention in the past decades [3], [23]. A great number of results on these topics have appeared in the literature. Among the different approaches dealing with these problems, the methods based on the concepts of *quadratic stability* and *quadratic stabilizability* have

Manuscript received March 28, 2003; revised July 17, 2003. Recommended by Associate Editor P. A. Iglesias. This work was supported in part by RGC HKU 7103/01P, the Foundation for the Author of National Excellent Doctoral Dissertation of China under Grant 200240, and the National Science Foundation under Grants 60304001 and 60074007.

S. Xu is with the Department of Automation, Nanjing University of Science and Technology, Nanjing 210094, P. R. China.

J. Lam is with the Department of Mechanical Engineering, University of Hong Kong, Hong Kong.

Digital Object Identifier 10.1109/TAC.2003.822854